Engineering Co. for providing the sulfonated polystyrene ionomer. Thanks are also due to Philip E. Gibson for suggesting the Debye–Bueche model and to Soichi Wakatsuki for help with the ASAXS experiments. This work was supported by the U.S. Department of Energy under Contract DE-FG02-84ER45111. R.A.R. wishes to thank S.C. Johnson & Son and the Fannie and John Hertz Foundation for support. The Stanford Synchrotron Radiation Laboratory is supported by the Department of Energy, Office of Basic Energy Sciences, and the National Institutes of Health, Biotechnology Resources Program, Division of Research Resources.

References and Notes

(1) Wilson, F. C.; Longworth, R.; Vaughan, D. J. *Polym. Prepr. (Am. Chem. Soc., Div. Polym. Chem.)* **1968**, *9*, 505.
(2) Marx, C. L.; Caulfield, D. F.; Cooper, S. L. *Macromolecules* **1973**, *6*, 344.
(3) Fujimura, M.; Hashimoto, T.; Kawai, H. *Macromolecules* **1981**, *14*, 1309.
(4) Weiss, R. A.; Lefelar, J. A. *Polymer* **1986**, *27*, 3.
(5) Williams, C. E.; Russell, T. P.; Jérôme, R.; Horrion, J. *Macromolecules* **1986**, *19*, 2877.
(6) Gierke, T. D.; Munn, G. E.; Wilson, F. C. *J. Polym. Sci., Polym. Phys. Ed.* **1981**, *19*, 1687.
(7) Yarusso, D. J.; Cooper, S. L. *Polymer* **1985**, *26*, 371.
(8) Kumar, S.; Pinéri, M. *J. Polym. Sci., Polym. Lett. Ed.* **1986**, *24*, 1767.
(9) MacKnight, W. J.; Taggart, W. P.; Stein, R. S. *J. Polym. Sci., Polym. Symp.* **1974**, *45*, 113.
(10) Yarusso, D. J.; Cooper, S. L. *Macromolecules* **1983**, *16*, 1871.
(11) Ramaseshan, S., Abrahame, S. C., Eds. *Anomalous Scattering*; International Union of Crystallography: Copenhagen, 1975.
(12) Wagner, C. N. J. *J. Non-Cryst. Solids* **1980**, *42*, 3.
(13) James, R. W. *The Optical Principles of the Diffraction of X-Rays*; Cornell University: Ithaca, NY, 1965.
(14) Phillips, J. C.; Hodgson, K. O. In *Synchrotron Radiation Research*; Winick, H., Doniach, S., Eds.; Plenum: New York, 1980.
(15) Waseda, Y. *Novel Application of Anomalous X-Ray Scattering for Structural Characterization of Disordered Materials*; Springer-Verlag: New York, 1984.
(16) Stuhrmann, H. B. *Adv. Polym. Sci.* **1985**, *67*, 123.
(17) Lye, R. C.; Phillips, J. C.; Kaplan, D.; Doniach, S.; Hodgson, K. O. *Proc. Natl. Acad. Sci. U.S.A.* **1980**, *77*, 5884.
(18) Miake-Lye, R. C.; Doniach, S.; Hodgson, K. O. *Biophys. J.* **1983**, *41*, 287.
(19) Fairclough, R. H.; Miake-Lye, R. C.; Stroud, R. M.; Hodgson, K. O.; Doniach, S. *J. Mol. Biol.* **1986**, *189*, 673.
(20) Makowski, H. S.; Lundberg, R. D.; Singhal, G. H. U.S. Patent 3 870 841, 1975, to Exxon Research and Engineering Co.
(21) Lundberg, R. D.; Makowski, H. S.; Westerman, L. U.S. Patent 4 014 847, 1977, to Exxon Research and Engineering Co.
(22) Hubbard, S. R. Ph.D. Thesis, Stanford University, 1987.
(23) Bonse, U.; Hartmann-Lotsch, I. *Nucl. Instrum. Methods Phys. Res., Sect. A* **1984**, *222*, 185.
(24) Kronig, R. de L. *J. Opt. Soc. Am. Rev. Sci. Instrum.* **1926**, *12*, 527.
(25) Kramers, H. A. *Atti Congr. Fisici*, Como **1927**, 545.
(26) Suortti, P.; Hastings, J. B.; Cox, D. E. *Acta Crystallogr., Sect. A: Found. Crystallogr.* **1985**, *A41*, 417.
(27) Aur, S.; Kofalt, D.; Waseda, Y.; Egami, T.; Chen, H. S.; Teo, B.-K.; Wang, R. *Nucl. Instrum. Methods Phys. Res., Sect. A* **1984**, *222*, 259.
(28) Hosemann, R.; Bagchi, S. N. *Direct Analysis of Diffraction by Matter*; North-Holland: Amsterdam, 1962.
(29) Percus, J. K.; Yevick, G. *Phys. Rev.* **1958**, *110*, 1.
(30) Wertheim, M. S. *Phys. Rev. Lett.* **1963**, *10*, 321.
(31) Thiele, E. *J. Chem. Phys.* **1963**, *39*, 474.
(32) Fournet, G. *Acta Crystallogr.* **1951**, *4*, 293, 587.
(33) Kinning, D. J.; Thomas, E. L. *Macromolecules* **1984**, *17*, 1712.
(34) Yarusso, D. J. Ph.D. Thesis, University of Wisconsin—Madison, 1983.
(35) Handlin, D. L.; MacKnight, W. J.; Thomas, E. L. *Macromolecules* **1981**, *14*, 795.
(36) Debye, P.; Bueche, A. M. *J. Appl. Phys.* **1949**, *20*, 518.
(37) Debye, P.; Anderson, H. R.; Brumberger, H. *J. Appl. Phys.* **1957**, *28*, 679.
(38) Clough, S. B.; Cortelek, D.; Nagabhushanam, T.; Salamone, J. C.; Watterson, A. C. *Polym. Eng. Sci.* **1984**, *24*, 385.
(39) Eisenstein, A.; Gingrich, N. S. *Phys. Rev.* **1942**, *62*, 261.

Neutron and X-ray Scattering Studies on Semicrystalline Polymer Blends

T. P. Russell* and H. Ito

IBM Research, Almaden Research Center, 650 Harry Road, San Jose, California 95120-6099

G. D. Wignall

Oak Ridge National Laboratory, Oak Ridge, Tennessee 37830.
Received September 19, 1987; Revised Manuscript Received December 8, 1987

ABSTRACT: Mixtures of poly(ethylene oxide), PEO, with protonated or deuteriated poly(methyl methacrylate), PMMAH or PMMAD, respectively, crystallized at 50 °C have been investigated by small-angle X-ray scattering, SAXS, and small-angle neutron scattering, SANS. It is shown that PMMA is incorporated into the amorphous phase between the crystalline lamellae. In addition, the thickness of the crystalline lamellae remains constant as a function of temperature which is in keeping with a small interaction parameter between the PEO and PMMA. The diffuse-phase boundary between the crystalline and amorphous phase is ca. 15 Å greater for the SAXS measurements than that measured by SANS. These results suggest the existence of a region on the crystal surface in which the crystalline order dissipates and from which the noncrystallizable PMMA is excluded.

Introduction

The morphology in mixtures of semicrystalline and amorphous polymers develops from a balance between kinetic and thermodynamic factors. In particular, the rate of crystal growth will depend upon the temperature at which the crystallization occurs in relation to the glass transition temperature and the equilibrium melting point. In the case of mixtures, the specific interactions between the two polymers and the cooperative diffusion coefficient will also play key roles in the development of the morphology. For example, the amorphous component in mixtures of semicrystalline and amorphous polymers can reside between the crystalline lamellae or be excluded from the interlamellar amorphous phase yet be incorporated within the spherulitic structure or even be rejected, partially or completely, from the spherulite forming a matrix in which the spherulites are embedded. The first case has been clearly demonstrated with mixtures of poly(ϵ-caprolactone) with poly(vinyl chloride)[1] and poly(vinylidine fluoride), PVF_2, with poly(methyl methacrylate), PMMA,[2]

0024-9297/88/2221-1703$01.50/0

where the crystalline lamellae were shown by small-angle X-ray scattering SAXS to separate in order to accommodate the amorphous component. The second has been shown in the mixtures of isotactic polystyrene with atactic polystyrene.[3] In this case, a coarsening of the spherulitic texture was found yet the crystal–crystal separation distance remained constant. Finally, Keith and Padden[4,5] observed a partial exclusion of a low molecular weight diluent in mixtures of high and low molecular weight poly(ethylene oxide), PEO. Thus, a wide spectrum of morphologies is possible with semicrystalline-amorphous polymer mixtures, and a proper evaluation of properties of the mixtures requires an in-depth understanding of the different structures.

Recently, we investigated the crystallization kinetics in semicrystalline-amorphous polymer mixtures, in particular, mixtures of PEO with PMMA, using optical microscopy.[6] In this study, a theory was proposed that described the kinetics of crystal growth over a wide range of crystallization temperatures, composition, and molecular weights of the two components. While this treatment was quite successful in reducing the observed growth rates to a master curve, there were several assumptions made that were necessary in order to quantitatively describe the observed growth rate. These were that the Flory–Huggins interaction parameter χ_{AB} was effectively zero and that the amorphous component, i.e., PMMA, was incorporated between the crystalline PEO lamellae. The first of these assumptions has recently been discussed and has been shown by small-angle neutron scattering, SANS, to be quite reasonable.[7] It is the intent of this article to address this latter assumption by small-angle X-ray scattering, SAXS, and SANS.

SAXS which is insensitive to electron density variations in the sample and SANS which probes spatial correlations of the neutron scattering length should provide identical information in terms of the separation distance of crystalline lamellae. The need for both techniques arose initially from a resolution question. As will be shown, the small-angle long period, i.e., the center-to-center distance of the crystalline lamellae increased dramatically as PMMA was added to the PEO such that by 70% PEO instrumental resolution limited further investigation. SANS which is capable of higher instrumental resolution, due primarily to the longer wavelengths, provided complimentary information for the higher PMMA concentrations. The combination of SANS and SAXS, as will be shown, proved unequivocally that PMMA was incorporated between the crystalline lamellae. For those mixtures that were ammenable to study by both SANS and SAXS, a most unusual observation was made. As will be discussed the long period measured by SAXS and SANS were in quantitative agreement. However, the diffuse-phase boundary measured by SANS was ca. 15 Å less than that measured by SAXS, indicating the existence of an interfacial zone that is comprised of an essentially amorphous PEO region from which the amorphous PMMA was excluded. (This result supports the arguments made by Wendroff et al.[8,9] on the PVF_2/PMMA and the observations by Alfonso and Russell[6] on PEO/PMMA mixture where a concentration-independent relaxation not associated with the crystalline phase was observed in the semicrystalline mixtures.) The existence of such an interfacial zone has been suggested,[8,9] and we feel that the results presented here quantitatively show its presence and may reflect the generality of this behavior.

Experimental Section

The samples investigated in this study were mixture of PEO and PMMA crystallized from the melt at 50 °C for 96 h and then slowly cooled to room temperature. The PEO, a size exclusion chromatography standard (TSK standard PEO produced by Toyo Soda Manufacturing Co., Limited), was purchased from Polymer Laboratories having molecular weight of 145 000 with an M_w/M_n = 1.04. The protonated PMMA, referred to as PMMAH, was purchased from Polymer Laboratories and had a molecular weight of 129 000 with an M_w/M_n of 1.15. The deuteriated PMMA, referred to as PMMAD, was synthesized with a molecular weight of 136 000 and an M_w/M_n = 1.05. A full description of the synthesis and characterization of the tacticity of the PMMA has been reported previously.[7] The mixtures were prepared by dissolving preweighed quantities of the homopolymers in benzene warmed to 40 °C. After dissolution, the solution was cooled, frozen in liquid nitrogen, and warmed to 0 °C in a water/ice slurry, whereupon the benzene was freeze-dried. The remaining diaphanous powder was pressed in a pellet mold at room temperature and then transferred to a melt press where a pellet of a predesigned diameter and thickness was molded at 120 °C under pressure. The pellets, sandwiched between quartz windows with a ring of Teflon serving as a spacer, were placed under vacuum at room temperature for 24 h and then heated to 100 °C under vacuum to remove bubbles and voids. The specimens were then rapidly transferred to another vacuum oven preheated to 50 °C where they were allowed to crystallize under vacuum for 96 h.

SANS measurements were conducted at the National Center for Small Angle Scattering Research located at the Oak Ridge National Laboratory.[10] Experiments were performed at sample to detector distances of 15, 5, and 1.25 m by using neutrons of wavelength λ = 4.75 Å ($\Delta\lambda/\lambda$ = 0.06). Collimation of the neutron beam was achieved with 1.0- or 1.2-cm pinholes. At the shorter sample to detector distances beam guides were used to enhance the flux on the sample. SANS profiles for the mixtures at a sample to detector distance of 15 m were placed on an absolute level by using a series of secondary standards.[11] All other SANS data were normalized to the 15-m data by correcting the scattering profiles for changes in the scattering volume and solid angles subtended by the detector elements.

SAXS measurements were performed on a Kratky camera by using a 60-μm entrance slit and Ni-filtered Cu radiation. X-rays were supplied by a sealed source generator operated at 40 kV and 20 mA using a standard focus X-ray tube. The scattered X-rays were detected by a TEC Model 210 linear position sensitive proportional counter situated 0.63 m from the specimen. A single channel analyzer in the gating circuit of the detector was used to electronically discriminate the scattered radiation. The data were stored on a Tracor Northern TN-1750 prior to transfer to the host computer for processing. Typically, 24 h were allowed to collect a SAXS profile to obtain a satisfactory signal-to-noise ratio. The scattering profiles were desmeared by the methods outlined by Vonk et al.,[12] as well as by the method outlined by Strobl[13] taking into account the geometries of the incident beam profile and the detector. Good agreement was obtained between the two techniques. SAXS data were placed on an absolute level by using a secondary standard previously calibrated in our laboratory.[14]

Preliminary Data Reduction

Prior to analysis, both the SAXS and SANS data were corrected for electronic noise, detector homogeneity, and parasitic scattering. Of interest to this particular study is the coherent scattering arising from the periodic contrast variation (electron density in the case of SAXS and scattering length density in the case of SANS) in a direction normal to the surface of the lamellae. This requires the elimination of incoherent scattering for SANS and thermal density fluctuation scattering for both SAXS and SANS. Both these contributions to the scattering give rise to a constant level of scattering. At high scattering vectors, $q = (4\pi/\lambda) \sin(\epsilon/2)$ where ϵ is the scattering angle, these two contributions dominate the scattering and, therefore, can be eliminated by evaluating the slope of a Iq^4 versus q^4 plot. An example of such a plot for a 70% PEO/30% PMMAD SANS profile is shown in Figure 1. As can be

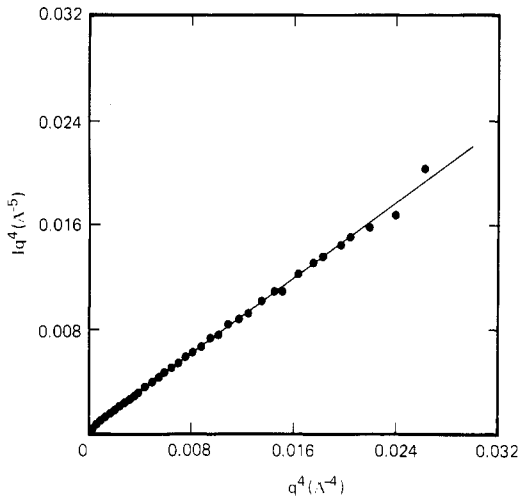

Figure 1. Plot of Iq^4 versus q^4 of the neutron scattering data obtained for a 70% PEO mixture with 30% perdeuterio PMMA. The slope of least-squares fit of the data at the higher scattering vectors yields the amount of background scattering to be subtracted from the data. For the neutron scattering, this represents the contributions arising from incoherent scattering and thermal density fluctuations, whereas for the X-ray scattering data only the latter comprises the background.

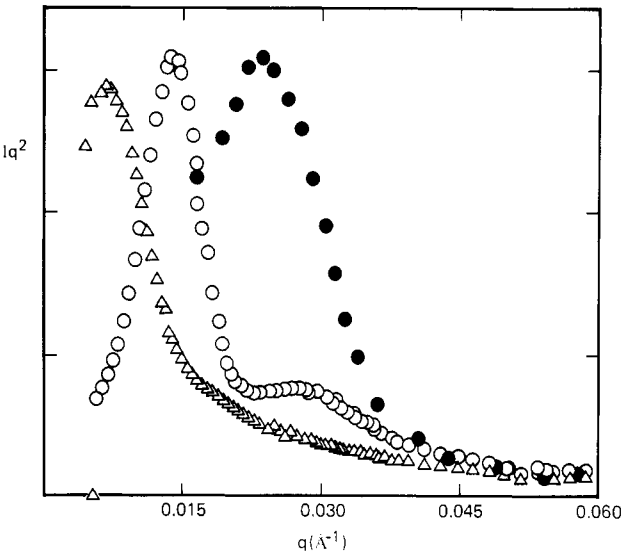

Figure 2. Intensity as a function of the scattering vector for mixtures of PEO with PMMA. The pure PEO data (●) were obtained by X-ray scattering, whereas those for the 70% (○) and 50% (△) PEO mixtures were obtained by small-angle neutron scattering. The shift in the long period to smaller scattering vectors is clearly evident in these data.

seen, very good linear behavior for $q^4 > 0.08$ Å^{-4} ($q \gtrsim 0.54$ Å^{-1}) was observed for these data. Similar behavior was found for the other mixtures by both SANS and SAXS. Consequently, the fluctuation scattering and incoherent scattering were easily eliminated from the data. It should be noted that this method is approximate in that there must be a small contribution to the magnitude of the slope arising from the coherent scattering. However, this overcorrection represents only a small fraction (less than 1%) of the total scattering and will be well within the experimental uncertainties of the measurements. When the analysis of the higher scattering vectors is of interest, care must be taken so that this overcorrection does not introduce artifacts.

Results and Discussion

A series of Lorentz-corrected scattering profiles for PEO and its mixture with PMMA crystallized at 50 °C for 96 h are shown in Figure 2. The data represent results of both SAXS and SANS experiments. For the pure PEO and its mixtures with PMMA down to 75 wt % PEO SAXS provided a facile means of characterizing the morphology. However, due to the limited spatial resolution of the instrument, the scattering profiles of the 70% and 50 wt % PEO mixtures could only be measured accurately by SANS. In those cases, the PMMA mixed with the PEO was perdeuteriated providing the maximum contrast between the crystalline and amorphous phases. From the results in Figure 2, there are several important pieces of information that can be derived from a cursory inspection of the scattering profiles. First, as was discussed by Silverstre et al.,[15] the position of the peak maximum shifts to smaller scattering vectors. From the peak position, using Bragg's law, the long period or the average center-to-center distance between adjacent similar phases can be obtained. These are shown in Figure 3 for all the compositions studied as a function of the weight fraction of PEO. As can be seen, the long period increases with the addition of PMMA, indicating that the PMMA is being incorporated between the crystalline lamellae. It is important to note that the SAXS and SANS long periods increase smoothly with no discontinuity between the two results. For the SAXS experiments, the crystalline phase

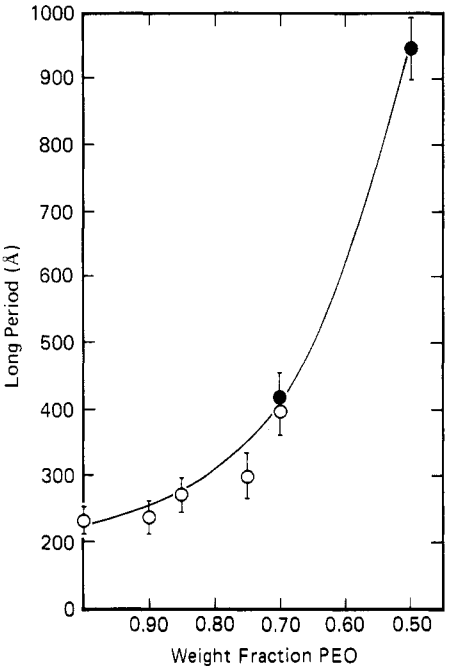

Figure 3. Long period as a function of the weight fraction of PEO. Plotted on this curve are results from X-ray (○) and neutron (●) scattering measurements. Due to the instrumental resolution of the X-ray camera, it was not possible to obtain precise data on the identical samples at higher PMMA concentrations where SANS showed a pronounced reflection.

has the higher electron density or contrast factor, whereas for the SANS experiments, the deuteriated PMMA makes the scattering length density of the amorphous phase higher. If and only if the PMMA is being incorporated between the crystal lamellae, then the two results should be measuring the same average distance. According to Babinet's reciprocity theorem, it does not matter which phase has the higher contrast since the intensity represents the square of the scattering length density difference. These data alone, without further analysis, prove unequivocally that some of the PMMA resides between the crystalline lamellae. It should also be noted that the long period does not increase linearly with concentration. As

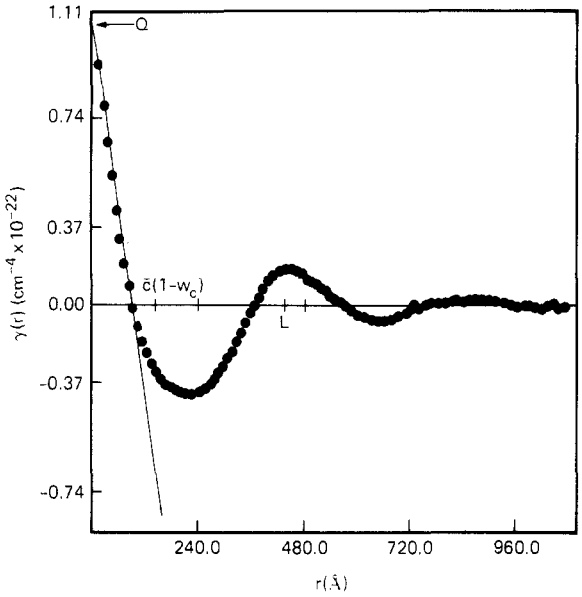

Figure 4. Correlation function for a 70% PEO mixture with perdeuterio PMMA. The correlation function was calculated from the SANS data by using the method of Strobl and Schneider.[16] Indicated in this are the average long period L, the invariant Q, and the average amorphous thickness $\bar{A}$.

can be seen from these data, the addition of 30% of PMMA increases the long period by ca. 70 Å. However, increasing the PMMA concentration further causes much more pronounced changes in the long period.

A second feature to be observed in these data is that for the pure PEO, only a single reflection is observed. In fact, only a single reflection was observed down to 75% by weight of PEO. However, for the 70% PEO sample, a second-order reflection is clearly evident, and then for the 50% PEO specimen, the second-order reflection is lost. The absence of the second-order reflection for the PEO is a strong indication that the linear crystallinity for the PEO is on the order of 50% and the second order is absent due to symmetry, whereas for the 70% mixture, the linear crystallinity has dropped substantially below this level. Increasing the concentration of PMMA further introduces sufficient disorder into the lamellar stucking so that higher order reflections are damped.

From either the SANS or SAXS data, the correlation function $\gamma(r)$ can be calculated without correction for deviations from Porod's law due to diffuse-phase boundaries in a manner outlined by Strobl et al.[16,17] In particular

$$\gamma(r) = \frac{1}{2\pi^2}\int_0^\infty q^2 I(q) \cos(qr)\, dq \qquad (1)$$

The correlation function for the SANS data of the 70% PEO in Figure 1 is shown in Figure 4. The shape of $\gamma(r)$ directly yields several important pieces of information. First, extrapolation of the linear portion of $\gamma(r)$ at small values of r to $r = 0$, the so-called "self-correlation triangle", yields the total integrated scattering or invariant Q. Provided the diffuse-phase boundary between the crystalline and amorphous phase is smaller than the average crystal thickness, there exists a linear region in $\gamma(r)$ over which this extrapolation can be made. This, of course, can be also obtained directly from the scattering data by,

$$Q = \int_0^\infty q^2 I(q)\, dq \qquad (2)$$

provided the data has been corrected for diffuse-phase boundaries. However, for arguments to be presented later, it was desirable not to perform this correction. Second,

Table I
Correlation Function Results[a]

wt fractn PEO	L, Å	$\bar{A}$, Å	$\bar{C}$, Å	E, Å	ϕ_c[b]
1.0	230	85	145	22	0.63
0.9	240	104	136	24	0.56
0.85	270	145	125	21	0.46
0.75	300	155	145	21	0.48
0.70	400	257	143	23	0.36
0.70	420	283	137	6	0.33
0.50	945	795	150	5	0.15

[a] L is the long period determined from the maximum in the Lorentz corrected scattering profile. $\bar{A}$ is the average thickness of the amorphous phase. $\bar{C}$ is the average thickness of the crystalline phase. E is the width of the diffuse phase boundary. [b] ϕ_c was determined from differential scanning calorimetry using ΔH_u for PEO of 47.0 cal/g.[19]

the intercept of the self-correlation triangle at $\gamma(r) = 0$ yields $\bar{C}(1 - w_c)$ where $\bar{C}$ is the average crystal thickness and w_c is the linear crystallinity. In principle, if the scattering length density of the amorphous phase is known and the system contains two phases, the base of the self-correlation triangle can be drawn as a horizontal line at $-w_c(b_c - b_a)^2$, where b_c and b_a are the scattering length densities of the crystalline and amorphous phases, respectively. Considering arguments to be presented momentarily, it is not likely that either of these assumptions are valid. Thus, the average crystalline- and amorphous-phase thicknesses were obtained by multiplying the first maximum in the correlation function by w_c or $1 - w_c$, respectively, where w_c is the volume fraction of crystallinity as determined by differential scanning calorimetry. The average thickness of the crystalline, $\bar{C}$, and amorphous, $\bar{A}$, phases obtained in this manner are shown in Table I. One striking feature of these data is that over the entire composition range, the thickness of the crystalline phase remains constant. To within experimental errors, a similar result was obtained by Silvestre et al.[15] although their results show a slight increase in crystal thickness at lower PEO concentrations. This result further emphasizes the fact that the interaction parameter between PEO and PMMA is quite small as found previously.[7] If this were not the case, then the crystal thickness would be expected to increase at lower PEO concentrations due to a melting point depression. No evidence was found for such behavior in this study. A second feature of these data is that, down to PEO concentrations of 75%, the amorphous-phase thickness is less than 160 Å. For the PMMA used in this study, a typical value of the radius of gyration of PMMA is 103 Å.[7] This mandates that the PMMA be compressed between the crystalline lamellae since it cannot assume a random coil configuration in this confined space. This aspect has not been addressed in semicrystalline polymer mixtures. For PEO concentrations less than 75%, the amorphous-phase thickness is large enough to circumvent this issue. It is clear from these data that the addition of PMMA causes an increase in the thickness of the amorphous-phase, further demonstrating that PMMA is incorporated between the crystalline lamellae.

An interesting difference is observed between the neutron and X-ray scattering results. Examination of the initial portions of the correlation function for the SANS data given in Figure 4 shows that there are essentially no deviations from a linear behavior, whereas for the SAXS data a substantial deviation was observed. These results suggest that the interface between the crytalline and amorphous regions exhibit different characteristics depending upon the type of radiation used. Basically for the SANS case, the interface appears to be sharp, whereas for

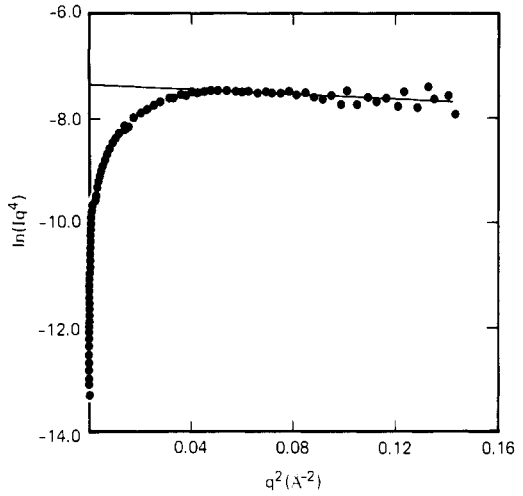

Figure 5. Porod plot of the SANS data for a 70% PEO mixture with 30% perdeuterio PMMA. The slope of the linear least-squares fit of the data at higher scattering vectors yields the thickness of the transition zone between the crystalline and amorphous regions. The deviations of these data from a simple q^{-4} dependence of the intensity represented a transition zone thickness of only several angstroms.

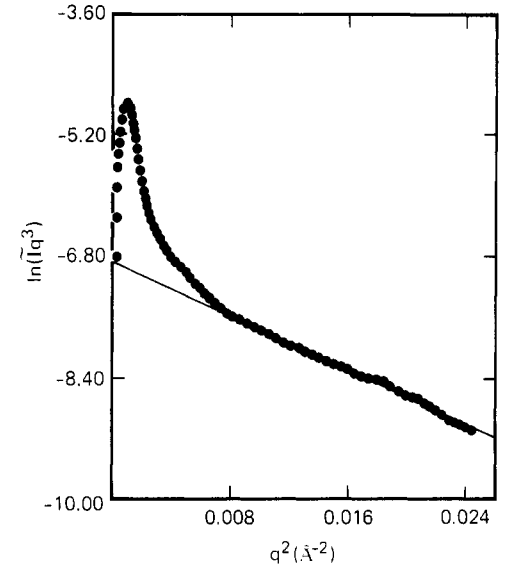

Figure 6. Porod plot of the smeared SAXS data for a 90% PEO mixture with proteo PMMA. The slope of the line from the data at higher scattering vector yields the thickness of the interface between the crystalline and amorphous regions. Deviations from Porod's law for the X-ray data indicate a diffuse-phase boundary of several tens of angstroms.

SAXS a diffuse interface is observed.

To investigate this question further, a Porod analysis was performed on both sets of data. As discussed by several authors,[19-24] the slope of a plot of ln (Iq^4) versus q^2 for desmeared or pinhole scattering data or ln ($\tilde{I}q^3$) versus q^2 for smeared intensities will yield the width of the transition zone between regions of different scattering length densities. Plots of this type are shown in Figure 5 for the SANS from a 50% PEO specimen and in Figure 6 for the SAXS from an 85% PEO specimen. Analysis of the smeared SAXS data was done so as to minimize treatment of the data in the high-angle range where the scattering is inherently weak. As can be seen, the data at high angles are accurately given by a straight line from which the diffuse-phase boundary, E, can be obtained. These are tabulated in Table I and are plotted in Figure 7 as a function of composition. In keeping with the correlation function analysis, the diffuse-phase boundary as

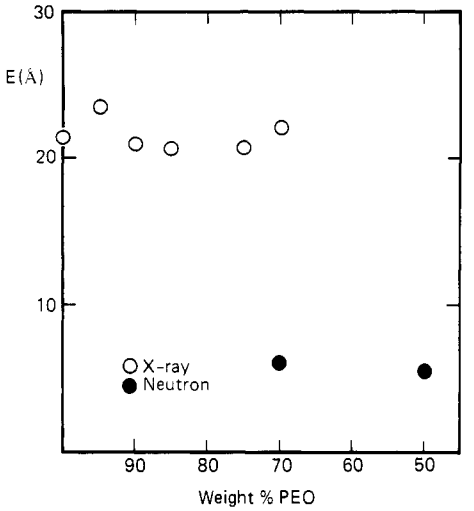

Figure 7. Thickness of the diffuse phase boundary as a function of composition as measured by SANS (○) and SAXS (●). Note that the SAXS and SANS values remain constant as the composition is varied; however, there is nearly a 15-Å difference between the two results. X-ray measurements were not possible on the 50% PEO sample since the long period was well outside the resolution of the instrument.

measured by SANS is very narrow, whereas that measured by SAXS is significantly broader. At the one concentration of overlap, i.e., at 70% PEO, this difference is striking. To within the experimental uncertainties of ±5 Å, the interface thickness is independent of concentration.

One possible explanation for this observation has recently been proposed by Hahn et al.[8,9] and Stein et al.[25] based on concepts developed by Mandelkern et al.[26,27] and Flory et al.[28] Basically, despite favorable interactions that may occur between two components in semicrystalline polymer mixtures, there exists an interphase between the crystalline phase and the mixed, amorphous phase that is comprised of the amorphous component of the crystalline polymer. Within this interphase, the order from the crystalline lamellae dissipates and the noncrystallizable component is excluded. The observation in the PVF_2 mixtures with PMMA of a dielectric relaxation characteristic of the pure, amorphous PVF_2[8] and the SAXS invariant[9] was used to support these arguments. Previously, we had also reported the observation of a dielectric relaxation in the semicrystalline PEO/PMMA mixtures[6] that occurred at temperatures near the T_g of the PEO. Down to 50% by weight of the PEO, this relaxation changed very little with composition; however, the strength of the relaxation was weak in the mixtures. This result and the observed differences in the interface thickness measured by SANS and SAXS suggest that a similar type of interphase may be present in the PEO/PMMA mixtures.

Consider the schematic diagrams in Figure 8 which depict the electron density and neutron scattering lengths of a semicrystalline PEO/PMMA mixture. Beginning with the electron density of the crystalline PEO, $\rho_{c,PEO}$, we proceed in a direction normal to the surface of the lamellae. Exiting the crystal, the order is lost causing a drop in the electron density. After sufficient order has been lost, which for PEO is on the order of 15 Å, the PMMA begins to mix with the PEO and forms a mixture between the lamellae with an electron density of $\rho_{a,PEO+PMMA}$. These steps are then reversed as we proceed from the mixed, amorphous phase to the next lamella and so forth. In terms of neutron scattering length density the situation is somewhat different. Since PEO is protonated, the scattering length density of the crystalline PEO, $b_{c,PEO}$, is small due to the negative scattering length of the protons. As we exit the

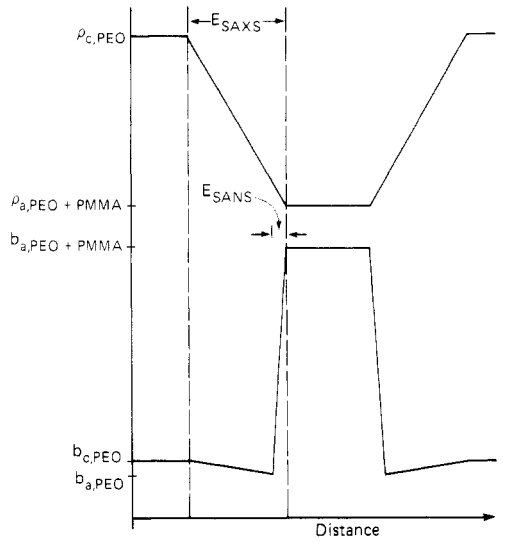

Figure 8. Schematic diagram of the electron density (upper) and the neutron scattering length density (lower) as a function of distance in a direction normal to the surface of the lamellae. The area between the dashed lines represents the transition zone between the crystalline lamellae and the homogeneous amorphous mixture. E_{SAXS} and E_{SANS} are the thicknesses of the interface as measured by SAXS and SANS, respectively.

crystal, the scattering length density decreases further approaching that of the amorphous PEO, $b_{a,PEO}$. As the deuteriated PMMA mixes with the PEO, the scattering length density increases dramatically to that of the amorphous, interlamellar mixture, $b_{a,PEO+PMMA}$. As with the electron density, progressing to the next lamella reverses the steps. The drop in the neutron scattering length density from the crystalline to amorphous PEO is negligible in comparison to the change from the crystalline PEO to that of the mixture. Now, in the diagram, the effective interface measured by SAXS and SANS is indicated, and, as shown, the interface as measured by SAXS is much greater than that measured by SANS. This is precisely what is observed experimentally and, thus, provides a reasonable interpretation of the observed differences.

In the case of PEO/PMMA, this interphase between the crystalline phase and the amorphous PEO/PMMA mixture between the lamellae must have a density that continuously decreases from the crystalline density to account for the two different values of E observed. The distance over which this interphase exists is also less than the length of the unit cell of PEO in the chain direction which is 19.3 Å.[29] Thus, for these mixtures, this interphase simply represents a region at the crystal surface where the crystalline order is lost. The exclusion of the PMMA arises simply from a packing consideration since the order from the crystalline phases must be sufficiently low to allow mixing. The previous observation of a weak, concentration-independent relaxation[6] may or may not be associated with this interphase region since the size scale is relatively small and it may be questioned whether or not the PEO chains can be considered as truly amorphous.

Finally, the total integrated scattering or the invariant Q measured experimentally can be compared to calculations based on a simple two-phase model or a three-phase model taking into account the existence of the observed interphase region. For a two-phase system

$$Q = \overline{(\Delta\rho)^2} = \phi_1\phi_2(\rho_1 - \rho_2)^2 \quad (3)$$

and for a three-phase system

$$Q = \overline{(\Delta\rho)^2} = \phi_1\phi_2(\rho_1 - \rho_2)^2 + \phi_1\phi_3(\rho_1 - \rho_3)^2 + \phi_2\phi_3(\rho_2 - \rho_3)^2 \quad (4)$$

Table II
Integrated Scatterings

wt % PEO	$10^{-22}Q_m$,[b] cm^{-4}	$10^{-22}Q$,[c] cm^{-4}	$10^{-22}Q_m$,[d] cm^{-4}
100	7.99	7.99	7.99
90	8.43	7.51	7.88
85	7.31	7.42	7.74
75	6.38	7.05	7.42
70	5.73	6.79	7.25
70	1.05	1.21	17.70
50	0.0038	0.0013	0.0023

[a] Values of the invariant are reported in cm^{-4} which for X-rays is related to the mean square fluctuation in the electron density by $i_e N^2(\Delta\rho)^2$ where i_e is the Thomson scattering factor and N is Avogardro's number and for neutrons is given by $\overline{(\Delta b)^2}$. [b] Experimental values. [c] Calculated for a two-phase model. [d] Calculated for a three-phase model.

where $\overline{(\Delta\rho)^2}$ is the mean square scattering length density difference and ρ_i is the scattering length density of phase i with volume fraction ϕ_i. If, as a limiting case, we assume that the mixed, amorphous phase is homogeneous and that the interphase has a scattering length density equal to that of amorphous PEO, then the results given in Table II are found. Along with these data are shown the experimentally evaluated invariants. It is clear from these data that both models predict the observed trends in the concentration dependence of the invariant; however, the calculated invariants for both models are somewhat high. In addition to this, it is evident that the invariants calculated for these two models are not sufficiently different to allow differentiation between the two models. Thus, the data in Table II only allow us to say that trends in the measured invariants show clearly that PMMA is incorporated between the crystalline, PEO lamellae.

In conclusion, the results presented in this study show unequivocally that the amorphous PMMA is incorporated between the crystalline PEO lamellae. The invariant of the thickness of the lamellae strongly suggests that the interaction parameter between PEO and PMMA is quite small. Finally there is a 15-Å discrepancy between the width of the diffuse-phase boundary as measured by SAXS and SANS, the former being larger, which supports the idea that there is an interfacial region at the surface of the PEO crystals from which the amorphous PMMA is excluded. The width of this interface is less than one unit cell thickness of the PEO, suggesting that this interface for the PEO represents a volume over which the order from the crystals is lost.

Registry No. PEO, 25322-68-3; PMMAH, 9011-14-7; neutron, 12586-31-1.

References and Notes

(1) Russell, T. P.; Stein, R. S. *J. Polym. Sci., Polym. Phys. Ed.* **1983**, *21*, 999.
(2) Morra, B. S. Ph.D. Thesis, University of Massachusetts at Amherst, Massachusetts, 1980.
(3) Warner, F. P.; Stein, R. S.; MacKnight, W. J. *J. Polym. Sci., Polym. Phys. Ed.* **1977**, *15*, 2113.
(4) Keith, H. D.; Padden, F. J. *J. Appl. Phys.* **1963**, *34*, 2409.
(5) Keith, H. D.; Padden, F. J. *J. Appl. Phys.* **1964**, *35*, 1270.
(6) Alfonso, G. C.; Russell, T. P. *Macromolecules* **1986**, *19*, 1143.
(7) Ito, H.; Russell, T. P.; Wignall, G. D. *Macromolecules* **1987**, *20*, 2213; *Mater. Res. Soc. Symp. Proc.* **1987**, *79*, 87.
(8) Hahn, B. R.; Wendorff, J.; Yoon, D. Y. *Macromolecules* **1985**, *18*, 718.
(9) Hahn, B. R.; Herrmann-Schönherr, O.; Wendorff, J. H. *Polymer* **1987**, *28*, 201.
(10) Koehler, W. C. *Physica* **1986**, *137B*, 320.
(11) Wignall, G. D.; Bates, F. S. *J. Appl. Crystallogr.* **1987**, *20*, 28.
(12) Vonk, C. G.; *J. Appl. Crystallogr.* **1975**, *8*, 340.
(13) Strobl, G. R. *J. Appl. Crystallogr.* **1973**, *6*, 365.

(14) Russell, T. P. *J. Appl. Crystallogr.* **1983**, *16*, 473.
(15) Silvestre, C.; Cimmino, S.; Martuscelli, E.; Karasz, F. E.; MacKnight, W. J. *Polymer* **1987**, *28*, 1190.
(16) Strobl, G. R.; Schneider, M. *J. Polym. Sci., Polym. Phys. Ed.* **1980**, *18*, 1340.
(17) Strobl, G. R.; Schneider, M.; Voigt-Martin, I. *J. Polym. Sci., Polym. Phys. Ed.* **1980**, *19*, 1361.
(18) Van Krevelen, D. W. *Properties of Polymers*; Elsevier: Amsterdam, 1976.
(19) Porod, G. *Kolloid-Z.* **1951**, *124*, 83.
(20) Porod, G. *Kolloid-Z.* **1952**, *125*, 51.
(21) Porod, G. *Kolloid-Z.* **1952**, *125*, 108.
(22) Ruland, W. *J. Appl. Crystallogr.* **1971**, *4*, 70.
(23) Vonk, C. G. *Appl. Crystallogr.* **1973**, *6*, 81.
(24) Koberstein, J. T.; Morra, B. S.; Stein, R. S. *J. Appl. Crystallogr.* **1980**, *13*, 34.
(25) Herman, W.; Stein, R. S. *Bull. Am. Phys. Soc.* **1987**, *32*, 876.
(26) Popli, R.; Mandelkern, L. *Polym. Bull. (Berlin)* **1983**, *9*, 260.
(27) Popli, R.; Glotin, M.; Mandelkern, L. *J. Polym. Sci., Polym. Phys. Ed.* **1984**, *22*, 407.
(28) Flory, P. J.; Yoon, D. Y.; Dill, K. A. *Macromolecules* **1984**, *17*, 868.
(29) Tadokoro, H.; Chatani, Y.; Yoshihara, T.; Tahara, S.; Murahashi, S. *Makromol. Chem.* **1964**, *73*, 109.

The Microstructure of Block Copolymers Formed via Ionic Interactions†

T. P. Russell*

IBM Research, Almaden Research Center, 650 Harry Road, San Jose, California 95120-6099

R. Jérôme, P. Charlier, and M. Foucart

Laboratory of Macromolecular Chemistry and Organic Catalysis, University of Liège, 4000 Liège, Belgium. *Received October 6, 1987; Revised Manuscript Received December 7, 1987*

ABSTRACT: The morphology produced by solution cast mixtures of telechelic polymers end capped with tertiary amine functionalities with telechelic polymers terminated with either sulfonate or carboxylate moieties closely resembles that seen in block copolymers formed by covalent bonding of two dissimilar chain segments. It has been found by temperature-dependent small-angle X-ray scattering and optical microscopic studies that the sulfonate/tertiary amine associations are more stable at elevated temperatures than the carboxylate analogs. These effective block copolymers undergo a classic order/disorder transition at elevated temperatures similar to that seen in covalently bonded block copolymers. However, due to the nature of the ionic associations, as the order/disorder is approached, the width of the interface between the two phases remains sharp. Finally, by increasing the molecular weight of the telechelic polymers at temperatures above the order/disorder transition temperature, the effects of an upper critical solution temperature are seen. Here, the telechelic polymers appear to phase separate in a spinodal manner. The phase diagrams for these systems are dictated by the relative positions of the microphase separation temperature of the effective block copolymers, the upper critical solution temperature of the dissociated telechelic polymers, the temperature at which the ionic aggregates dissociate, and the glass transition temperature.

Introduction

The miscibility of two homopolymers is more the exception than the rule. Typically, phase separation exhibited by two polymers occurs on a size scale of several microns which gives rise to opacity and can cause a deterioration of properties due to poor interfacial adhesion. These problems can be circumvented to some extent by copolymerizing the desired monomers. Copolymerization tends to make the two polymers more miscible by covalently linking the otherwise incompatable polymers, and it also limits the microphase separation to a size scale comparable to molecular dimensions.[1] An alternate approach to the copolymerization route is to place proton donating end groups on one polymer and proton accepting moieties on the other homopolymer.

Previously, the phase separation of two immiscible polymers was modified by ionic interactions via a proton transfer from the acid end groups of one polymer to the tertiary amine end groups of a second polymer.[2] Infrared spectroscopic studies showed that proton transfer from carboxylic acid end groups to the dimethylamino end groups occurred with formation of ammonium carboxylate ion pairs.[2,3] The solution viscosity of the related telechelic polymer blends in a common, nonpolar solvent was also significantly modified by the ionic bonding between the two polymers and possible electrostatic interactions of the ammonium carboxylate ion pairs.[3] Optical microscopy has shown it is possible to obtain homogeneous mixtures on a scale of ca. 0.2 μm, depending on the nature, molecular weight, and functionality of the immiscible polymers, and the strength of the ion pairs (ammonium carboxylates or sulfonates).[3] Finally, two distinct glass transition temperatures (T_g) for the acid and tertiary amine telechelic polymer mixtures were observed which indicated that these mixtures are actually microphase separated in a manner that is analogous to block copolymers.[3] These results strongly suggest that mixtures of the acid and tertiary amine telechelic polymers form essentially a multiblock copolymer in the bulk where phase separation is restricted to the molecular level.

In this paper small-angle X-ray scattering (SAXS) studies on mixtures of amine-terminated polyisoprene with carboxylic acid terminated poly(α-methylstyrene) will be presented. It is shown that the morphologies of these

†The work reported herein was partially done at Stanford Synchrotron Radiation Laboratory which is supported by the Department of Energy of Basic Energy Sciences and the National Institute of Health, Brotechnology Resource Program, Division of Research Resources.

0024-9297/88/2221-1709$01.50/0